Microstrip Elliptic Function Filters Using the Novel Miniaturized Edge-coupled Split Ring Resonators

Suk-Hyung Jang and Jong-Chul Lee
RFIC Research and Education Center, Kwangwoon University
447-1 Wolgye-dong, Nowon-ku, Seoul 139-701, Korea
TEL) +82-2-940-5203, FAX) +82-2-918-6381
E-mail: jclee@kw.ac.kr

1. Introduction

In modern microwave communication systems, the filter characteristic such as the circuit size, the selectivity, and the insertion loss might be one of the critical issues. From the conventional half-wavelength hairpin resonator to the latest split ring resonator, optimum developments of the resonator have been achieved. In ref. [1-4], the elliptic function filter types can be realized using filters with cross couplings to give a number of alternative paths, which a signal may take between nonadjacent resonators. Depending on phase of a signal, the multi-path effect can provide attenuation poles at finite frequencies or group delay flattening, or even both simultaneously. They need only a few sections while Butterworth and Chebyshev filter types require more sections to achieve a sharp cut-off frequency response. Therefore, the microstrip elliptic filters show the advantages of high performance, low cost, and easy fabrication [5, 6]. In this paper, new applications of the novel miniaturized edge-coupled split ring resonators (NMEC-SRRs) which lead to cross-coupled elliptic function bandpass filters (CCEF BPFs) are introduced.

2. Basic Theory of the EC-SRR

Square and circular loops are widely used as elements for frequency selective surfaces and reflecting arrays. Since these loops are symmetrical, the scattering parameters are insensitive to polarization at normal incidence. However, the resonant frequency becomes a strong function of polarization when the conductor has opening at a suitable location. Fig. 1(c) shows the NMEC-SRR used in the design of CCEF BPFs in this paper while the conventional EC-SRR has a ring type [3, 4]. In Fig. 1(c), the NMEC-SRR can be designed with inserting the coupled lines into the loops as square type, which leads to size reduction without severe change of its characteristics compared with Fig. 1(b).

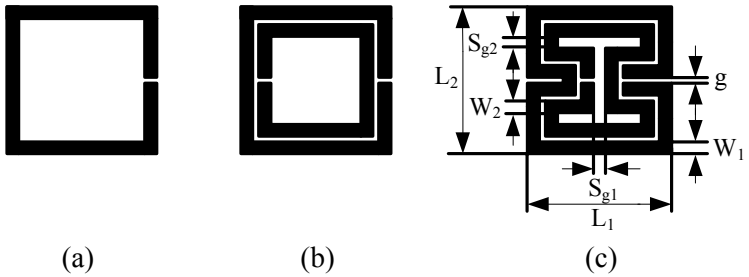

Fig. 1. Structural variations of open loop resonators (OLRs): (a) The capacitive loaded OLR, (b) The EC-SRR, and (c) The NMEC-SRR; Geometric parameters for the NMEC-SRR: W_1=W_2 =0.5, g=0.2, S_{g1}=0.5, S_{g2}=0.58, L_1=L_2 =6.16. All are in mm.

The equivalent circuit model of the NMEC-SRR in Fig. 1(c) is similar to that of conventional EC-SRR as shown in Fig. 2.

ISBN: 89-86522-78-0 94460©KEES

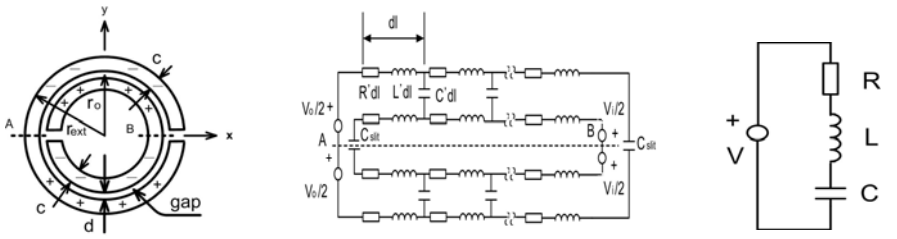

(a) (b) (c)

Fig. 2. Layout of the conventional EC-SRR and its equivalent circuits: (a) The EC-SRR structure (b) The completely equivalent circuit (c) The simplified equivalent circuit.

In Fig. 2 [3], the conventional EC-SRR consists of two open rings while the rings are identical and parallel to each other. It comprises two conductive rings printed on a thin dielectric substrate and separated by a narrow gap. Each ring has a slit, and the rings are arranged such that the slits are on the opposite sides of line of symmetry. The electrical dimensions of the EC-SRR are much smaller than a wavelength of the impinging plane wave. In Fig. 2(b), the voltage induced in the conventional EC-SRR in which two open rings are mutually coupled, can be simply calculated from Faraday's law:

$$V = -j\omega\mu_0 AH_i$$

Here, V is induced voltage, ω is radial frequency, and H_i is incident magnetic field, which is assumed being perpendicular to the loop. The symbol A and μ_0 are indicated to the loop area and free-space permeability, respectively. The induced voltages are modeled as simple voltage sources located at point A (the source V_0 — the outer ring) and point B (the source V_i — the inner ring). The completely equivalent circuit is sketched in Fig. 2(b). The symbol R' and L' stand for the distributed resistance and inductance, respectively. C_{slit} and C' represent the capacitance of the slits and the distributed capacitance of the gap between rings, respectively. From Fig. 2(b), two main loops (the inner and outer rings) which are connected across the gap via distributed capacitance C' can be identified. It is important to notice that voltage V_0 is always higher than voltage V_i by the ratio of areas formed by the outer and inner rings. Thus, current essentially flows from the outer ring into the inner ring across the gap. It flows through many branches formed by distributed capacitance C'. Due to this branching, the current in the outer ring changes depending on the location at the ring. Therefore, it is maximal at the point A, then decreases along the ring and reaches minimal value at the slit. All the currents which flow from the outer ring into the inner ring, contribute to the net current in the inner ring. In conclusion, the current in the inner ring exhibits the maximum at the location of voltage source V_i (point B), then decreases along the ring and reaches the minimum at the slit. If the current flowing across the slit would be negligible, the whole circuit can be simplified as shown in Fig. 2(c). The whole device then behaves as an LC circuit driven by an external electromotive force. The total capacitance of this LC circuit will be the series capacitance of the outer and the inner halves of the EC-SRR and the resonance frequency ω_0 is given by the capacitance per unit length between the rings and the total inductance of the EC-SRR. The above results for these polarities are confirmed by a more detailed electromagnetic analysis in [3, 4].

3. Design of the CCEF BPFs and Their Experiment Results

In the case of a four-pole CCEF BPF, the coupling coefficients (namely, the elements of coupling matrix, and input and output single-loaded external quality factor, Q_e) are found to be $K_{12}=K_{34}= 0.02694$, $K_{14}=-0.00468$, $K_{23}=0.02339$, $Q_{ei}=Q_{eo}=30.95$. For the case of a three-pole CCEF BPF, the coupling coefficients are found to be $K_{12}=K_{23}= 0.03308$, $K_{13}=-0.02012$, $Q_{ei}=Q_{eo}=22.58$, which are synthesized using the method described in [7]. These coupling coefficients can be quite

easily identified from the relationships between two split resonant frequencies used in the full-wave EM simulators. Also, the tapped-line feed is used for the loaded external quality factor, Q_e while the coupled-line feed can be applied.

The four-pole and three-pole CCEF BPFs using the NMEC-SRR are designed and fabricated for the demonstration. The proposed filters are fabricated on a dielectric substrate with a relative dielectric constant of 10.2 and a thickness of 1.524 mm. They are equally designed into the center frequency of 1.95 GHz and passband bandwidth of 3.077 %. The layout and dimensions of these filters are shown in Fig. 3.

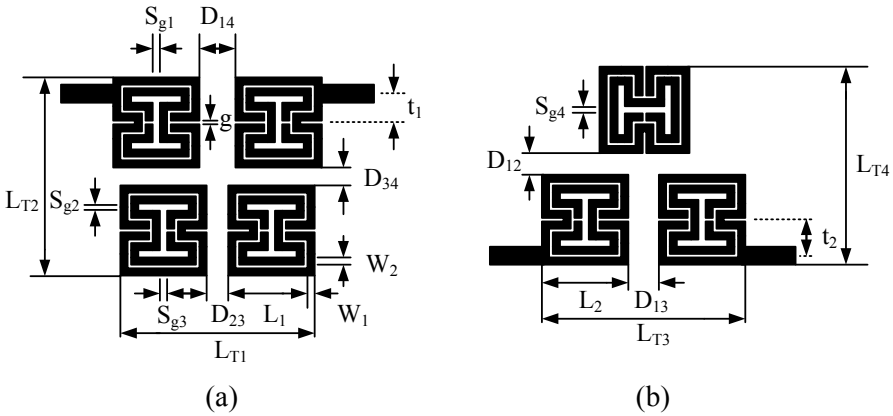

(a) (b)

Fig. 3. Configurations of the proposed microstrip miniaturized EC-SRR filters: (a) The four-pole cross-coupled elliptic function bandpass filter, (b) The three-pole cross-coupled elliptic function bandpass filter; Geometric parameters for each isolated resonator: S_{g1}=S_{g4} =0.5, S_{g2}=0.565, S_{g3}=0.38, L_1=5.63, L_2=6.11, g=0.2, t_1=2.04, t_2=2.36, D_{12}=0.55, D_{13}= 0.91, D_{14}=1.92, D_{23}=1.67, D_{34}=1.61, L_{T1}=0.236λ_{go}, L_{T2}=0.235λ_{go}, L_{T3} =0.222λ_{go}, L_{T4}=0.216λ_{go}. All are in mm.

To realize accurate center frequencies, they can be tuned with either the gap widths (between outer and inner resonators) or strip widths. The fabricated filters are measured with an HP 8510C vector network analyzer. The simulation and measurement results for the circuits are shown in Fig. 4.

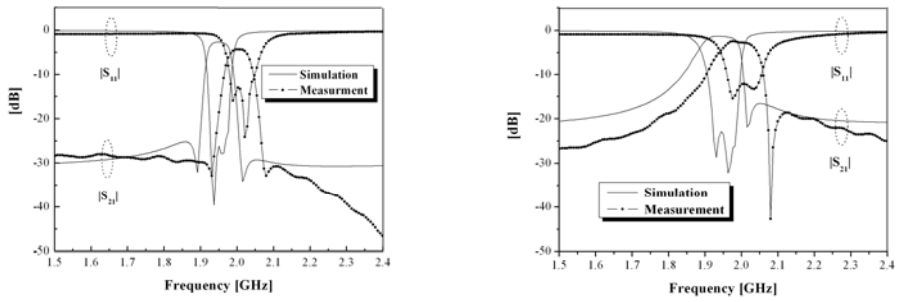

(a) (b)

Fig. 4. Simulation and measurement results for two filter types in Fig. 3: (a) The four-pole CCEF BPF, (b) The three-pole CCEF BPF

For the case of the four-pole CCEF BPF, the measured insertion loss is about 4.28 dB at the center frequency of 2.0 GHz, which is mainly resulted from the conductor loss while the simulated insertion loss is about 2.63 dB. The measured return loss is about 13.0 dB while the simulated return loss is about 26.10 dB. The difference between the simulation and measurement results is considered due to process error. The measured rejection is achieved in the design by replacing a pair of

attenuation poles at -81 MHz and 81.5 MHz from the center frequency, respectively while the simulated rejection is achieved by replacing a pair of attenuation poles at $f_0 \pm 61.5$ MHz.

On the other hand, for the case of the three-pole cross-coupled elliptic function bandpass filter, the measured insertion loss is about 2.77 dB at the center frequency of 2.0 GHz, while the simulated insertion loss is about 1.36 dB. The measured return loss is about 12.2 dB while the simulated return loss is about 23.53 dB. The measured rejection is achieved in the design by replacing an attenuation pole at 78 MHz from the center frequency while the simulated rejection is achieved by replacing an attenuation pole at 65 MHz from the center frequency. Although the center frequencies are a little shifted about 2.67 % in the frequency responses and there are some discrepancies in return losses, the measurement results for the four-pole and three-pole CCEF BPFs are well agreed with simulation data.

4. Conclusion

In this paper, new planar CCEF BPFs using the NMEC-SRRs have been introduced. Also, both the four-pole and the three-pole CCEF BPFs have been successfully demonstrated. Since the physical dimensions of the NMEC-SRR are much smaller than a signal wavelength, the proposed filters are extremely compact and can be used to reject parasitic frequencies in microstrip structures by simply patterning properly tuned EC-SRRs. With the characteristics of the capability of implementing attenuation poles, the compactness and flexibility in size, and the simplicity in both the design and fabrication, the CCEF BPFs using the NMEC-SRRs can be used as one of new elements in microwave systems.

Acknowledgement

This work has been performed through the Support Project of University Information Technology Research Center (ITRC) supported by the Ministry of Information & Communication of Korea.

References

[1] L. H. Hsieh and K. Chang, "Compact elliptic-function low-pass filters using microstrip stepped-impedance hairpin resonators," *IEEE Trans. Microwave Theory Tech.,* vol. 51, no. 1, pp. 193-199, Jan. 2003.

[2] J. T. Kuo and E. Shih, "Microstrip stepped impedance resonator bandpass filter with an extended optimal rejection bandwidth," *IEEE Trans. Microwave Theory Tech.,* vol. 51, no. 5, pp. 1554-1559, May 2003.

[3] R. Marques, F. Mesa, J. Martel, and F. Medina, "Comparative analysis of edge- and broadside-coupled split ring resonators for metamaterial design-theory and experiments," *Proc. IEEE Trans. Antennas and Propagation,* vol. 51, no. 10, pp. 2572-2581, Oct. 2003.

[4] S. Hrabar and J. Bartolic, "Simplified analysis of split ring resonator used in backward meta-material," *Proc. Int. Conf. Mathematical Methods in Electromagnetic Theory,* vol. 2, pp. 560-562, Sept. 2002.

[5] J. S. Hong and M. J. Lancaster, "Microstrip cross-coupled trisection bandpass filters with asymmetric frequency characteristics," *Proc. IEEE Antennas and Propagation,* vol. 146, no. 1, pp. 84-90, Feb. 1999.

[6] J. S. Hong and M. J. Lancaster, "Theory and experiment of novel microstrip slow-wave open-loop resonator filters," *IEEE Trans. Microwave Theory Tech.,* vol. 45, no.12, pp. 2358-2365, Dec. 1997.

[7] J. S. Hong and M. J. Lancaster, "Couplings of microstrip square open-loop resonator for cross-coupled planar microwave filters," *IEEE Trans. Microwave Theory Tech.,* vol. 44, no.12, pp. 2099-2109, Nov. 1996.

[8] J. S. Hong and M. J. Lancaster, *Microstrip Filters for RF/Microwave Aplications*, New York: John Wiley & Sons, 2001.